Proceedings of the 14th International Heat Transfer Conference
IHTC14
August 8-13, 2010, Washington, DC, USA

IHTC14-23083

AIR INGRESS ANALYSIS: COMPUTATIONAL FLUID DYNAMIC MODELS

Chang H. Oh* and Eung S. Kim
Idaho National Laboratory
Idaho Falls, ID.83415

ABSTRACT

Idaho National Laboratory (INL), under the auspices of the U.S. Department of Energy (DOE), is performing research and development that focuses on key phenomena important during potential scenarios that may occur in very high temperature reactors (VHTRs). Phenomena identification and ranking studies to date have ranked an air ingress event, following on the heels of a VHTR depressurization, as important with regard to core safety. Consequently, the development of advanced air-ingress-related models and verification and validation data are a very high priority.

Following a loss of coolant and system depressurization incident, air will enter the core of the High Temperature Gas Cooled Reactor through the break, possibly causing oxidation of the core and reflector graphite structure. Simple core and plant models indicate that, under certain circumstances, the oxidation may proceed at an elevated rate with additional heat generated from the oxidation reaction itself. Under postulated conditions of fluid flow and temperature, excessive degradation of lower plenum graphite can lead to a loss of structural support. Excessive oxidation of core graphite can also lead to a release of fission products into the confinement, which could be detrimental to reactor safety. Computational fluid dynamics models developed in this study will improve our understanding of this phenomenon.

This paper presents two-dimensional (2-D) and three-dimensional (3-D) computational fluid dynamic (CFD) results for the quantitative assessment of the air ingress phenomena. A portion of the results from density-driven stratified flow in the inlet pipe will be compared with the experimental results.

INTRODUCTION

Air-ingress scenarios and the physical mechanisms that dominate each stage were extensively investigated in this paper. The anticipated air-ingress scenario is shown in Figure 1. After a pipe break, coolant (helium) inside of reactor is first discharged out of the reactor vessel (Depressurization). After depressurization, air in the containment is intruded into the reactor vessel through the bottom part of the horizontal pipe forming stratified flow since the air and the helium have different densities (Stratified Flow (Stage 1)). After air fills the bottom of the reactor vessel, another counter-current flow occurs driven by temperature differences between the inside and outside of the vessel (Stratified Flow (Stage 2)). The basic physical mechanism of this process is the same as the previous stratified flow (Stage 1). However, in this process, density gradient is generated by temperature gradient. Therefore, this process does not stop because the inside and outside temperature gradient of the reactor vessel always exists during the air-ingress process. This convective flow will force the flow to move into the reactor core if it has enough energy to overcome it. If the intruded flow does not have enough energy to overcome the hydrostatic head of core fluids, the process will be dominated by a molecular diffusion process (Diffusion). Finally, if a buoyancy force is enough to generate the overall natural convection flow, a massive air-ingress begins.

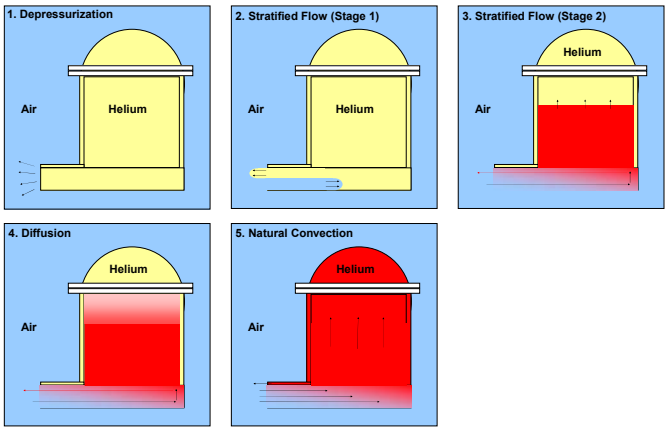

Figure 1. Air ingress scenario.

This paper focuses on the stratified flow process for both Stages 1 and 2, and estimates the dominant physical process for each stage by comparing time scales of different physical mechanisms.

3-D DEGB ANALYSES BY CFX CODE

A 3-D CFD analysis with CFX-12 was performed for the air ingress accident of the 600 MWth GT-MHR reactor under the assumption of a double-ended guillotine break (DEGB) in order to understand the air ingress behavior in detail and estimate the onset of natural circulation time. According to previous research, FLUENT 2-D results show that the onset of natural circulation time is about 200 seconds, which differs greatly from the 1-D GAMMA results of about 150 hours (Oh et al. 2008). The 1-D option of the GAMMA code was not able to capture the stratified flow and the flow recirculation in the lower plenum. The FLUENT 2-D analysis used a simplified porous model with a friction factor correlation and an approximated thermal equilibrium model to simulate the hydraulic resistance because of a friction and form loss and the heat transfer between the air and the solid structure in the lower plenum and the core block. The 3-D CFD analysis with the real grid model, especially for the lower plenum, was introduced to verify the 2-D FLUENT results.

The air ingress phenomenon is usually driven by the stratified flow (Liou et al. 2005) and the pressure build-up in the lower plenum during air heat-up and reduced inertia in the recirculation pattern. Air ingress may also be interrupted by the hydraulic resistance that takes place when the air passes a complicated geometry in the reactor. Therefore, it is not expected that an exactly simulated grid model for the complicated geometry of the lower plenum and core block can accurately predict the propagation of the air ingress inside the reactor. A grid interface function that connects two nonconformal meshes was used to complete the 3-D grid model because of the complicated nature of combining the consecutive mesh generation for the lower plenum, core blocks, and coolant riser within a single model.

The grid interface implemented in the CFX-12 (ANSYS 2009) is superior to that of other CFD codes (Kang 2006); however, the 3-D DEGB analysis by CFX-12 cannot simulate the helium blow-down phase with a decay heat generation in the core blocks. This is because CFX-12 has trouble obtaining fully converged solutions for the large pressure difference between the reactor and the confinement in the blow-down phase, and there is presently no implemented model for decay heat generation. The CFD calculations were therefore made at the pressure equalization between the confinement and the reactor vessel following the high pressure helium blow down to the confinement. The 3-D CFX analysis should therefore be carefully used to only predict the air ingress behavior because of the density driven stratified flow, buoyant flow by heat transfer, and hydraulic flow interrupted by complicated geometry. If the 3-D CFX analysis is able to predict the physical characteristics of an air ingress accident, the 3-D CFX analysis may also be used to find a mitigation method for the air ingress accident.

3-D GRID MODEL

In order to calculate the air inflow from the confinement into the reactor vessel through the broken pipes, a half symmetric grid model simulating the confinement and the reactor vessel internal was generated (see Figure 2) based on the design data of the 600 MWth GT-MHR (Oh et al. 2008). The inner and outer reflector was also modeled to simulate the solid heat structure and the flow path formed from the core block upper region to the coolant riser upper region in the air ingress accident. A hexahedral mesh was separately generated by ICEM-CFD software (ANSYS 2008) for all regions in the reactor and confinement except the lower plenum, and then all separated models were connected by using the grid interface function of CFX-12. The lower plenum grid model was initially generated by using GAMBIT with hexahedral, tetrahedral, and pyramidal meshes (Johnson 2008). It was transformed to the grid model for CFX-12 by ICEM-CFD.

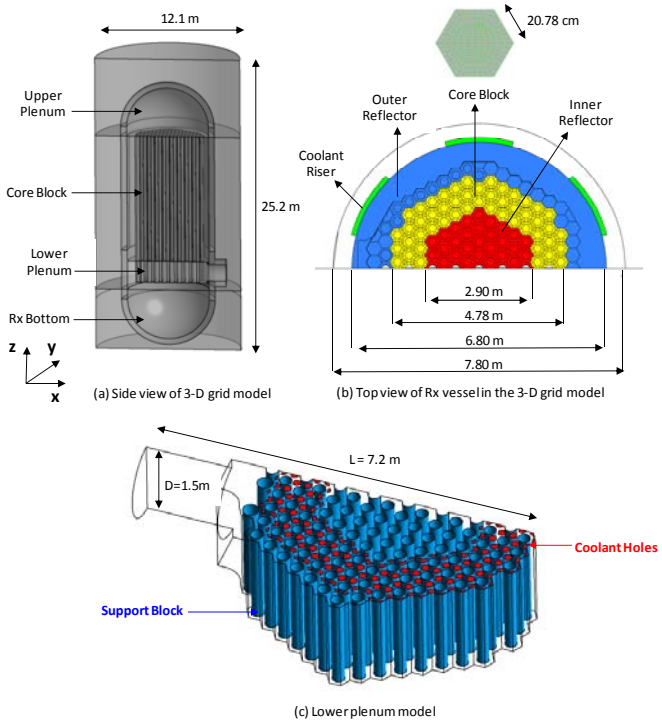

Figure 2. 3-D grid model for the DEGB analysis.

All meshes were densely distributed in a fluid region of the grid model, except the confinement, to prevent numerical diffusion and assure a low courant number (Equation (1)). About two million mesh cells were generated for all the core blocks to predict the air ingress more accurately because the expected flow regime in the core blocks is a buoyant flow caused by heat transfer between the core block walls and the air. The 2-mm bypass gaps between the core blocks were neglected to avoid the large number of cells required to resolve a 2-mm gap. The expected CFD results with the bypass gap are not expected to differ greatly from those without the bypass gap. A coarse mesh distribution was used in the confinement, except around

the broken pipes and the reactor vessel wall, because locally precise CFD results are not necessary for the regions far from the broken pipes and the reactor vessel walls. Thirty CFX parallel licenses are being used to compute the air ingress phenomena in the HTGR reactor and the confinement with a total of 8.5 million meshes.

$$\text{Courant Number} = V\Delta t / \Delta x \quad (1)$$

where

V = Fluid velocity (m/s)
Δt = Time step (sec)
Δx = Mesh length (m).

The shutdown cooling system located in the reactor bottom region and several guide tubes in the upper plenum were neglected in the grid model because the anticipated advantages of those models are not essential in predicting the air ingress from the confinement into the core blocks and the coolant riser. The detailed information of the mesh distribution and the geometry are shown in Table 1.

Table 1. Number of mesh and volume data for each region in the 3-D grid model.

Reactor Internal		Confinement
Core Blocks	Volume : 60.35 m^3 (Volume Porosity : 0.185) Height : 10.82 m Hexahedral mesh : 2,248,560	Volume : 961.05 m^3 Hexahedral mesh: 621,183 Fluid volume ration the confinement to the reactor internal: 3.81 Total meshes number : 8,517,835
Lower Plenum	Volume : 15.29 m^3 Height : 1.84 m Hexahedral mesh : 677, 917 Tetra mesh : 25,940 Pyramids mesh : 1,103	
Upper Plenum	Volume : 66.27 m^3 Radius : 3.4 m Hexahedral mesh : 712,023	
Coolant Riser	Volume : 6.98 m^3 (2.328 $m^3 \times 3$) Height : 9.87 m Hexahedral mesh : 287,820 (2.328 $m^3 \times 3$)	
Rx Bottom	Volume : 82.33 m^3 Hexahedral mesh : 651,963	
Reflector and Solid Regions	Volume : 204.58 m^3 Hexahedral mesh : 3,075,831	

INITIAL BOUNDARY, POROUS MEDIA CONDITIONS AND PROPERTIES

This 3-D DEGB CFX analysis assumed that the helium discharge from the reactor into the confinement through the broken pipes is already complete and that global pressure equilibrium has occurred between the confinement side and inside the reactor. All initial conditions of the concentration, temperature, and pressure were computed using the GAMMA code, and those values were used in CFD calculations as initial conditions. This was done because a large computation time would be necessary to get a well converged solution for the helium blow-down phase.

Initial conditions (see Figure 3) for the air mass fraction, temperature, and pressure of the confinement and reactor, including the inner and outer reflectors, were given in accordance with the GAMMA and hand calculation results for the blow-down phase (Oh et al. 2008). The air mass fraction of 0.5 for the confinement was simply calculated by considering the pressure and volume difference between the confinement and the reactor with the ideal gas law during the blow-down phase. The initial pressure distribution along an elevation was automatically calculated by CFX-12 with a gravitational direction and a density value.

Based on the GAMMA results, a constant temperature condition (see Figure 4) for the wall boundary condition was applied along the core block walls, the surface of the core support block, and the surface of the reactor vessel. In the core wall temperature condition, the temperature of the core upper region (see Figure 4A) is lower than that of the core lower region (see Figure 4B) because the helium passes from the upper region into the lower region during normal operation. The constant wall temperature conditions may be verified because the solid structure temperature is not changed, at least for several minutes. The symmetric condition is also applied on the 180 degree cut plane of the grid model.

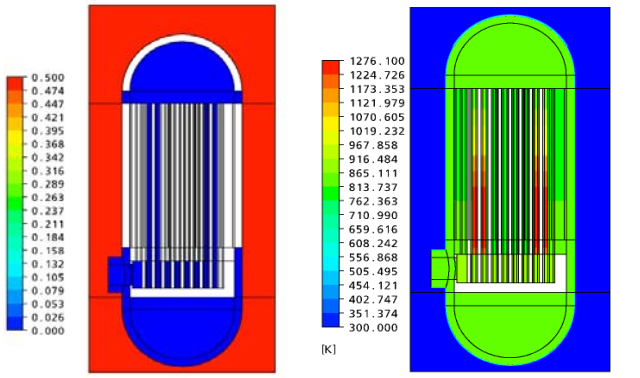

(a) Air mass Fraction (b) Temperature (K)

(Contours are plotted on the plane of y = 0.01m. Symmetry plane is y = 0.0 m)

Figure 3. Initial air mass fraction, temperature, conditions for 3-D CFX analysis.

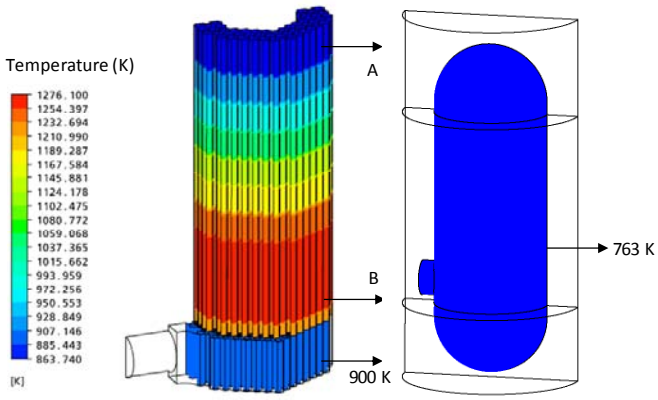

Figure 4. Wall temperature conditions for the core blocks, support blocks and reactor vessel.

A porous media condition was applied to the core blocks to simulate a pressure drop through the core blocks when helium or air flows along the core blocks. This was done to simulate 108 coolant channels with diameters of 12.7 and 15.8 mm per core block (Oh et al. 2008). The porous media condition was given in terms of a permeability (K_{perm}), a loss coefficient (K_{loss}), and a volume porosity (Equation (2)). The velocity (V_i) used in Equation (2) is a true velocity that can be obtained by dividing the superficial velocity with the volume porosity (Equation (3)). The true velocity concept of the porous media model may be important to the air ingress accident. The calculated turbulent viscosity based on the true velocity gradient can have an effect on the diffusion term of the species transport equation:

$$-\frac{\partial p}{\partial x_i} = \frac{\mu}{K_{perm}} V_i + K_{loss} \frac{\rho}{2} |V| V_i \qquad (2)$$

True Velocity = Superficial Velocity/Volume Porosity (3)

Experimental data are needed to give the accurate porous conditions simulating the core pressure drop under the air ingress accident because no other test data is available. Thus, conceptual design data regarding the core pressure drop (General Atomics 1996) at a normal operation condition were introduced to generate the porous condition values. A theoretically obtained porous condition should also be verified by the comparison of the calculated pressure drop values and the conceptual design data before applying it to the air ingress accident analysis. A steady-state calculation was performed using normal GT-MHR operating conditions (General Atomics 1996) to show the pressure drop of the core blocks and the reactor vessel from the cold duct to the hot duct. The calculated pressure distribution is shown in Figure 5 and the comparison results of the core pressure drop and reactor pressure drop between the conceptual design data and CFD results (Table 2) show good agreement (within 10%). Therefore, it is not possible to judge that these porous conditions may be used for the air ingress accident analysis.

The properties of the air and helium, such as thermal conductivity, molecular viscosity, and specific heat used for the 3-D CFX analysis, were cited from those of the FLUENT 2-D analysis, except for helium specific heat (ANSYS 2009).

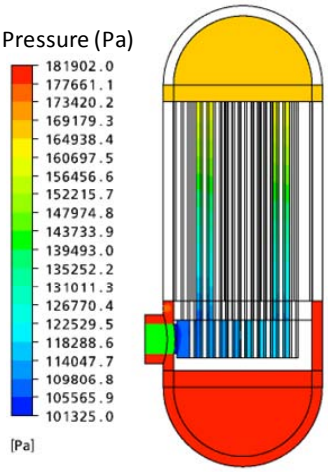

Figure 5. Pressure distribution results with the porous conditions under normal operating conditions.

Table 2. Pressure drop results using the porous media conditions.

Porous Conditions: • Volume porosity : 0.185 • Permeability : 9.706 × 10-4 m^2 • Resistance loss coefficient : 1.367 m^{-1}		
600 MWth GT-MHR Normal Operating Conditions [GA 2006]: • He mass flow rate : 320 kg/s • He average temperature through the core block : 743.65 K		
	Conceptual Design Data	CFD Results
Pressure drop of Rx vessel (Cold Duct to Hot Duct)	71 kPa	78.8 kPa
Pressure drop of active core	51 kPa	50.9 kPa

The National Aeronautics and Space Administration (NASA) format correlations in Table 3 were used for the helium specific heat property in the 3-D CFX analysis. The binary molecular diffusivity are shown in Figure 6. The air and helium density was obtained by the ideal gas law. The graphite properties for thermal conductivity and specific heat for the inner and outer reflectors were quoted from the FLUENT 2-D analysis.

FLOW FIELD MODELS AND NUMERICAL MODELS FOR THE 3-D CFX ANALYSES

The air ingress accident under the DEGB was treated as a convective flow, a compressible flow, a turbulent flow, a species flow, a buoyant flow, and a transient flow.

Table 3. NASA format correlation for specific heat of helium.

- $Cp / R = a1 + a2T + a3T^2 + a4T^3 + a5T^4$
- R = 2,077 [J/kg K] for helium
- Lower temperature = 300 [K], Midpoint temperature = 1,000 [K], Upper temperature = 5,000 [K]
- Lower interval coefficient:
  a1 = 0.02500000E+02 [], a2 = 0.0E+00 [K^{-1}], a3 = 0.0E+00 [K^{-2}], a4 = 0.0E+00 [K^{-3}],
  a5 = 0.0E+00 [K^{-4}], a6 = -0.07453750E+04 [K], a7 = 0.09153488E+01 []
- Upper interval coefficient:
  a1 = 0.02500000E+02 [], a2 = 0.0E+00 [K^{-1}], a3 = 0.0E+00 [K^{-2}], a4 = 0.0E+00 [K^{-3}],
  a5 = 0.0E+00 [K^{-4}], a6 = -0.07453750E+04 [K], a7 = 0.09153489E+01 []

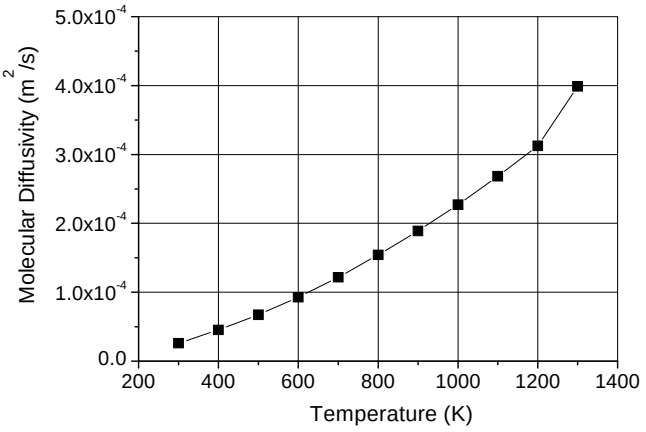

Figure 6. Binary diffusion coefficient between air and helium.

The governing equations, Equations (4)–(11), used in this study are the continuity, Navier-Stokes, energy, and species transport equations with a coupled solver algorithm (ANSYS 2009). Turbulent flow was modeled by the standard k-ε turbulent model with the scalable wall function, and the buoyancy flow was modeled by the density difference show in Equation (5) (ANSYS 2009). The governing equations used for the porous media are changed to Equation (11) by adding the volume porosity (λ) and area porosity tensor (*K*) into the general governing equations as follows:

$$\frac{\partial \rho}{\partial t} + \nabla \bullet \left(\rho \vec{V}\right) = 0 \tag{4}$$

$$\frac{\partial \left(\rho \vec{V}\right)}{\partial t} + \nabla \bullet \left(\rho \vec{V} \otimes \vec{V}\right) = -\nabla p + \nabla \bullet \left[\mu_{eff}\left(\nabla \vec{V} + \left(\nabla \vec{V}\right)^T\right)\right] + \left(\rho - \rho_{ref}\right)\vec{g} \tag{5}$$

$$\frac{\partial \left(\rho h_{tot}\right)}{\partial t} - \frac{\partial p}{\partial t} + \nabla \bullet \left(\rho \vec{V} h_{tot}\right) = \nabla \bullet \left(\lambda \nabla T + \frac{\mu_t}{\mathrm{Pr}_t}\nabla h\right) + \nabla \bullet \left(\vec{V} \bullet \tau\right) \tag{6}$$

$$\frac{\partial (\rho k)}{\partial t} + \nabla \bullet \left(\rho \vec{V} k\right) = \nabla \bullet \left[\left(\mu + \frac{\mu_t}{\sigma_k}\right)\nabla k\right] + P_k - \rho\varepsilon \tag{7}$$

$$\frac{\partial (\rho \varepsilon)}{\partial t} + \nabla \bullet \left(\rho \vec{V} \varepsilon\right) = \nabla \bullet \left[\left(\mu + \frac{\mu_t}{\sigma_\varepsilon}\right)\nabla \varepsilon\right] + \frac{\varepsilon}{k}\left(C_{\varepsilon 1} P_k - C_{\varepsilon 2}\rho\varepsilon\right) \tag{8}$$

$$\mu_{eff} = \mu + C_\mu \rho \frac{k^2}{\varepsilon} \tag{9}$$

$$\frac{\partial (\rho \phi)}{\partial t} + \nabla \bullet \left(\rho \vec{V} \phi\right) = \nabla \bullet \left(D_{AB} + \frac{\mu_t}{Sc_t}\right)\nabla \phi \tag{10}$$

$$\frac{\partial (\gamma \rho \phi)}{\partial t} + \nabla \bullet \left(\rho K \cdot \vec{V} \phi\right) - \nabla \bullet \left(\Gamma K \cdot \nabla \phi\right) = rS \tag{11}$$

where

$\vec{V}$	=	Velocity vector (m/s)
$\vec{g}$	=	Gravitation vector (m/s^2)
h_{tot}	=	Total enthalpy (J/kg)
D_{AB}	=	Binary diffusion coefficient (m^2/s)
k	=	Turbulent kinetic energy (m^2/s^2)
ε	=	Turbulent dissipation rate (m^2/s^3)
λ	=	Thermal conductivity (W/m K)
μ_{eff}	=	Effective viscosity (Pa sec)
ϕ	=	Variable
Γ	=	Diffusion coefficient.

The transient calculation for a total time of 80 seconds with a time step of 0.001–0.005 seconds was performed to carefully simulate the buoyant flow behavior because of the heat transfer from the solid structures into the air and helium. As a method of calculation, about 3–10 iterations were performed per the time step until the mass, enthalpy, and velocity residual of the air reached a value below 1.0×10^{-4}. The RMS Courant number was maintained below 2.5. The numerical models used for the 3-D CFX analysis are summarized as:

- Pressure-velocity coupling
- Linear equation solver: Algebraic Multigrid
- Convection scheme: Upwind 1st: $\phi_{ip} = \phi_{up}$
- Transient scheme: Backward Euler 1st: $\frac{\partial}{\partial t}\int_v \rho\phi dV = V\left(\frac{\rho\phi - \rho^o\phi^o}{\Delta t}\right)$
- Reynolds analogy: $Pr_t = 0.9$, $Sc_t = 0.9$
- 30 CPU parallel computation.

DISCUSSION ON THE CFD ANALYSIS RESULTS

The 3-D CFD results of the air ingress accident are shown in Figures 7–9. The air mass fraction contours according to time (see Figure 7) show the air inflow pattern from the confinement side into the reactor internal side. Figure 7 shows air entering into the hot and cold duct as soon as the CFD calculation starts. This is because the static head of the confinement side is slightly larger than that of the reactor internal side at the same elevation as much as the density difference between the air and the helium (see Figure 8(a) and (b)).

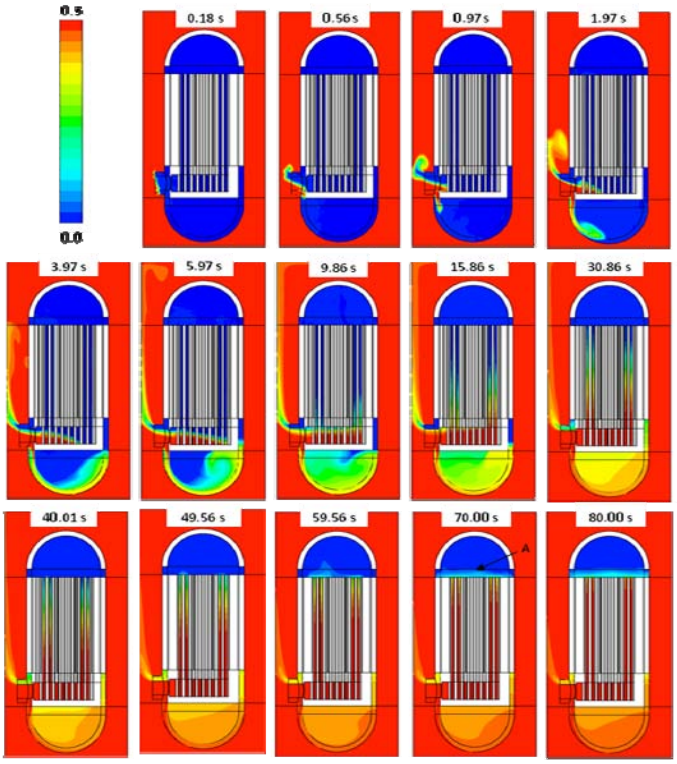

(Contours are plotted on the plane of y = 0.01m. Symmetry plane is y = 0.0 m)

Figure 7. Variation of the air mass fraction according to time.

Figure 8(a) shows the normalized pressure from the confinement (6.05 m from the center of the lower plenum) to the inlet point to the lower plenum (3.5 m from the center of the lower plenum) while z = 6.7 m represents the midpoint of the broken pipe height. The vertical line in Figure 8(a) is the pipe breach point and the curved line represents the curvature of the inlet pipe to the reactor vessel. Figure 8(b) shows a sudden density change at the breach point. Figure 8(c) shows the recirculation flow pattern at the breach point. Gravitational force directs the air inflow downward (see Figure 8(c)). Finally, an instability may be developed on the interface between the air and helium when the air flows into the helium by Rayleigh-Taylor instability (Lowe, Rottman, Linden 2005).

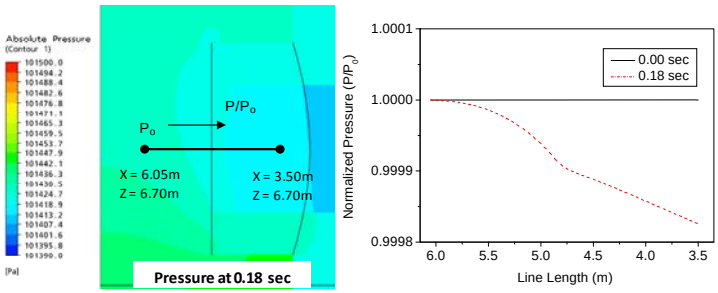

(a) Pressure contours and normalized pressure distribution along the line between x=6.05 m and x=3.50 m

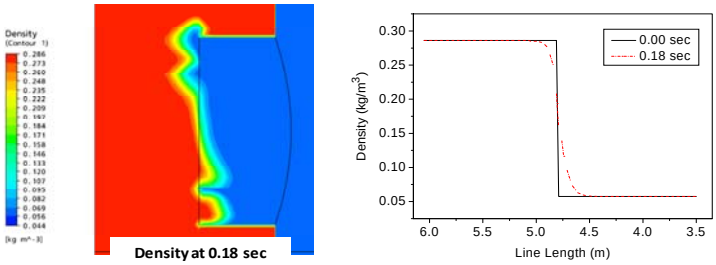

(b) Density contours and normalized density distribution along the line between x=6.05 m and x=3.50 m.

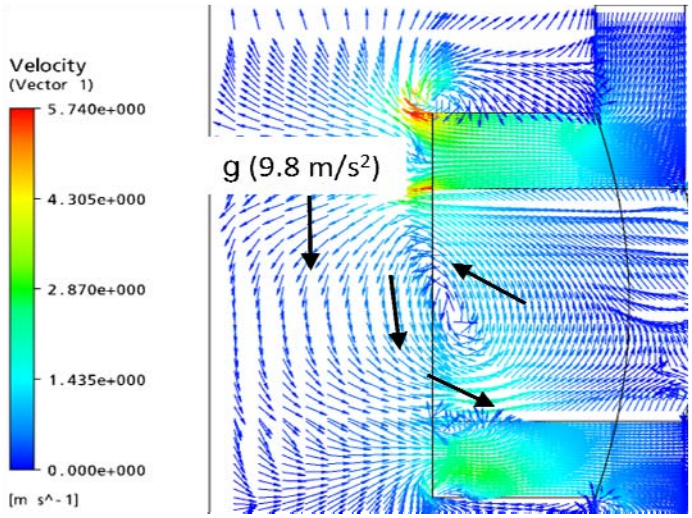

(c) Velocity profile on the plane of y = 0.01m at 0.18 seconds

(Contours are plotted on the plane of y = 0.01 m. Symmetry plane is y = 0.0 m)

Figure 8. Velocity profile, density, and pressure distribution at 0.0 seconds and 0.18 seconds.

As seen in Figure 7 above, the air arrives on the right end of the lower plenum at about 6 seconds and, after filling up the lower plenum and being heated by the support block, starts up into the core blocks right side at about 10 seconds. It takes approximately 50 seconds for the air in the lower part of the core block to move upward to the upper part by the buoyancy force generated by the density variation because of the heat transfer from the core block wall into the air. The air then arrives at the top of the coolant riser about 70 seconds after

filling up the volume of the upper plenum near the core upper region (see Figures 7 and 9A). The air that fills the upper plenum flows up through the reactor core, shown as two blank boxes in Figure 9. The air then moves downward along the coolant riser at about 80 seconds (see Figure 9A) and is also located at the lower part of the coolant riser (Figure 9B).

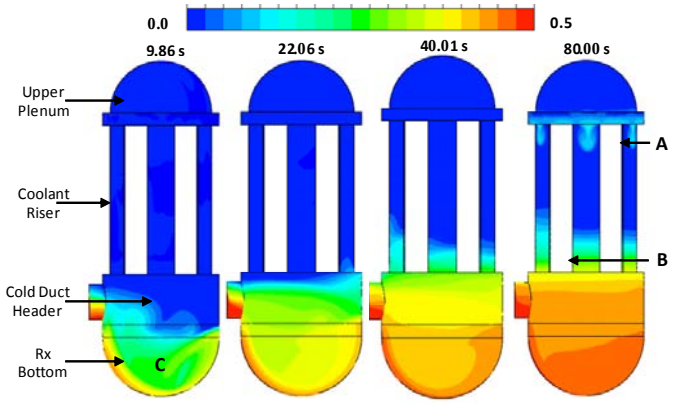

Figure 9. Air mass fraction of upper plenum, coolant riser, cold duct header, and reactor bottom.

It is believed that this air came from the confinement through the cold duct after filling up the reactor bottom region by gravitational force (see Figure 9C). From the air mass fraction contours, it can be expected that the air located on the upper region of the coolant riser can sufficiently reach the lower region of the coolant riser just 100–200 seconds after mixing with the air in the lower region.

Figure 10 shows the air mass fraction distribution on the hot and cold duct surface from a front viewpoint. The air flows into the cold duct header through the lower region of the broken cold duct at the same time the helium counter-current discharges through the upper region of the cold duct during the whole period. As time passes, the helium (blue color) in the helium discharge cold duct area steadily decreases.

Figures 11(a) and (b) show air mass fractions and velocity vectors in the lower plenum at 5.96 seconds. As can be seen, a portion of air velocity vector moves to the reactor core. When the flow is recirculated at the end of the plenum wall, it loses the momentum, resulting in pressure build-up, which makes the air move upward, if the hydrostatic force is less than the pressure build-up.

The rate at which the helium area decreases is proportional to the helium inventory volume in the reactor vessel and the velocity of the air inflow. In the hot duct side, the same situation of the counter-current flow driven by the density occurs just as on the cold duct side. The helium discharge through the upper region of the hot duct (see Figure 11(c)) continues until about 20 seconds. These different time scales

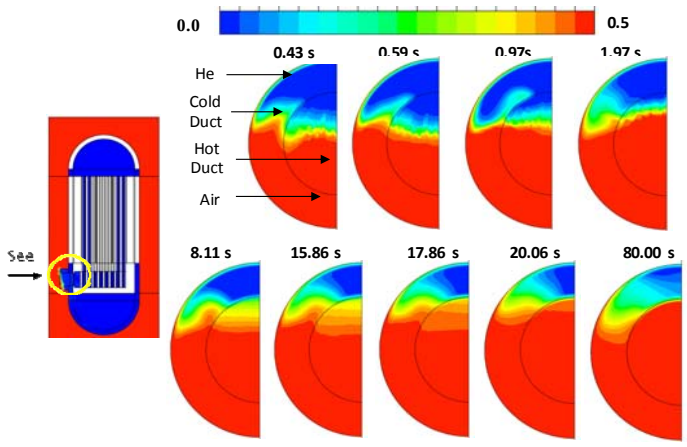

Figure 10. Air mass fraction of the hot and cold duct (front view).

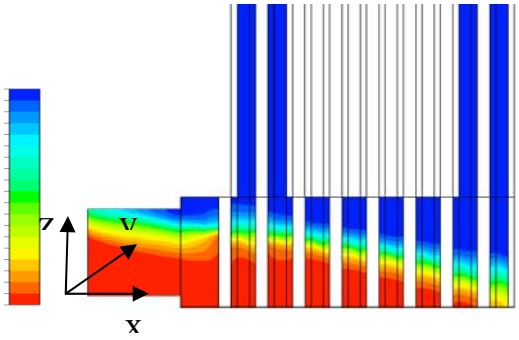

(a) Air mass fraction on plane of y = 0.01 m

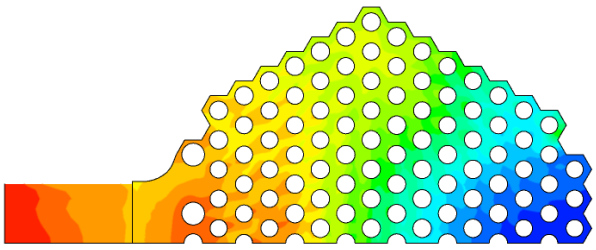

(b) Air mass fraction on plane of z = 1m from bottom of the lower plenum

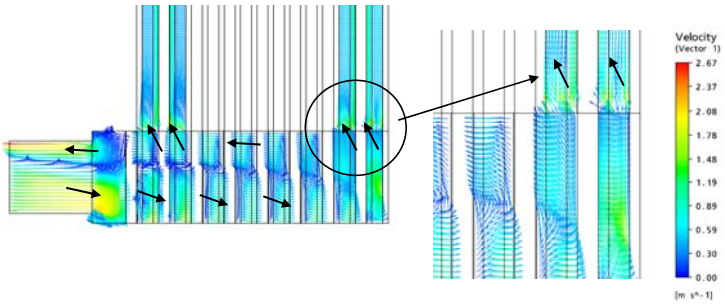

(c) Velocity profile on plane of y = 0.01 m

Figure 11. Air mass fraction and velocity profile in the lower plenum at 5.96 seconds.

for the discharge of helium through the cold and hot duct can be certified in terms of the volume averaged air mass fraction of the lower plenum, the reactor bottom, and the cold duct header as shown in Figure 12. The filling of the lower plenum with air is completed at about 20 seconds, whereas those of the reactor bottom and the cold duct are not completed until 80 seconds because the air through the cold duct moves downward and fills up the reactor bottom first.

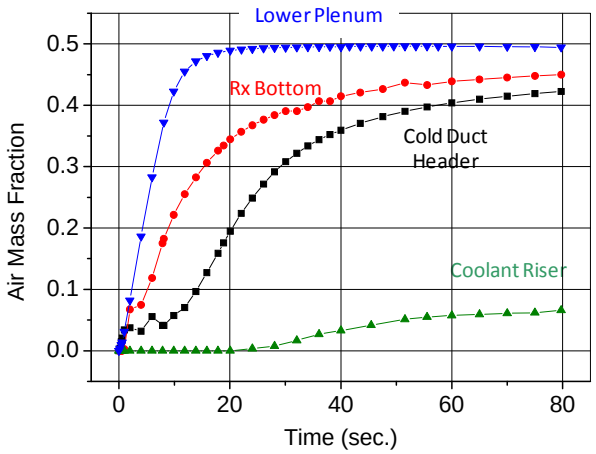

Figure 12. Volume averaged air mass fraction of the lower plenum, reactor bottom, cold duct header, and coolant riser (maximum value of the air mass fraction is 0.5).

The complete time of the helium discharge is very short when considering the lower plenum volume of 15.29 m^3 and the helium discharge velocity of about 1.0–2.67 m/s (see Figure 11). This situation may be caused from the helium located in the lower plenum at early stages that moves upward into the core blocks via natural circulation along the core blocks. The development of the helium natural circulation along the core block because of the initial temperature difference (see Figure 3(b)) may be confirmed in terms of the volume averaged velocity of the core block (see Figure 13). The velocity value shown in Figure 12 rapidly increases to about 1.1 m/s for 3.0–7.0 seconds, and then decreases to about 0.2 m/s at about 30 seconds. This natural circulation at an early stage may entrain the helium located in the lower plenum, and accelerate the helium circulation from the upper plenum region into the coolant riser.

Figure 14 shows the air mass fraction variation of the lower plenum, core, and core lower region according to time. An interested phenomenon is that the air mass fraction of the core starts to increase from about 10 seconds, even though about 80% of the lower plenum volume was already filled with air in the first 10 seconds. This may be caused by the discharging helium stream along the lower plenum upper region, thus preventing air penetration into the core blocks, or the air buoyancy force developed by the heat transfer from the support blocks being weak compared to the momentum of the helium discharging flow. It is possible to know, from the volume averaged temperature variation results of the lower plenum and the cold duct header (see Figure 15), that the starting time of the air flowing into the core block is closely related to the lower plenum temperature variation. The temperature graph of the lower plenum starts to increase at about 11 seconds from its continuous decreasing trend (see Figure 16(a)), whereas the temperature of the cold duct header steadily decreased to the end of the CFD calculation because it did not have the heat structure of the support block in the lower plenum.

The temperature increase from the decreasing trend can also be confirmed by the temperature contours at the plane of z = 6.7 m in the lower plenum (see Figure 16(g)). This may mean that the air heating time by the support block is an essential period for the air to have the buoyancy force because the buoyancy force can be developed by the density difference between a local value and an averaged value. It can therefore be expected that the starting time of the air flowing into the core block may be delayed if the air temperature of the lower plenum is maintained at a lower value.

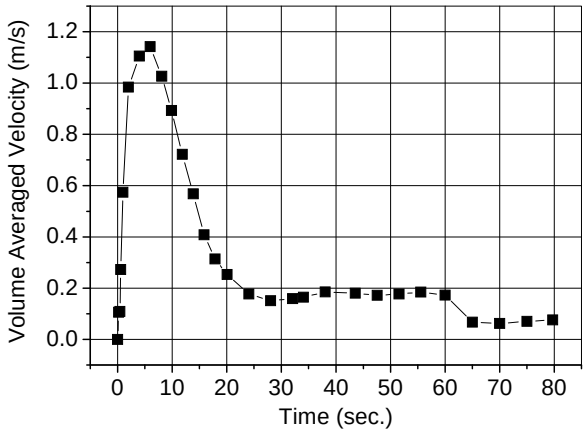

Figure 13. Volume averaged velocity of the core blocks.

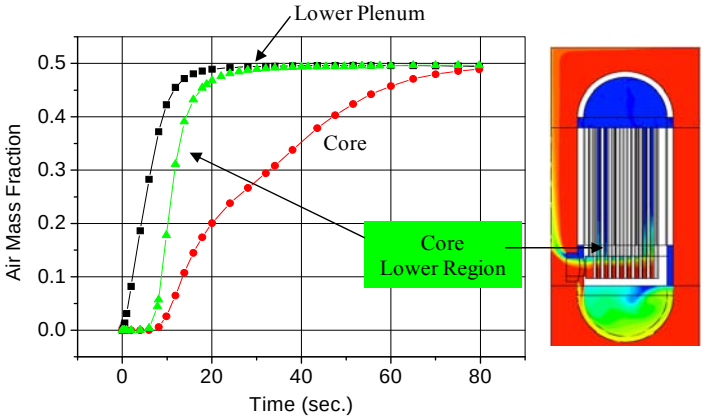

Figure 14. Volume and area averaged air mass fraction of the lower plenum, core blocks, and core inlet (maximum value of the air mass fraction is 0.5).

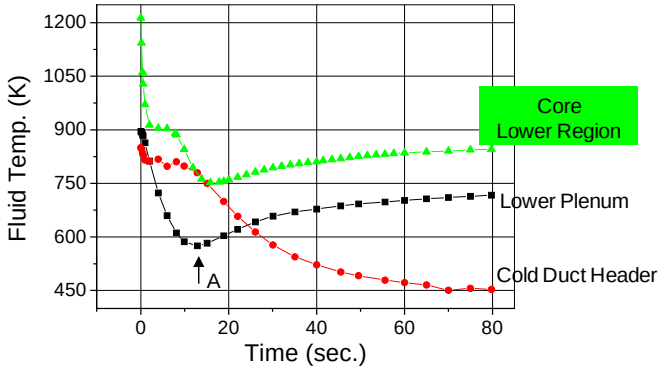

Figure 15. Volume and area averaged air temperature of the lower plenum, core blocks, and core inlet.

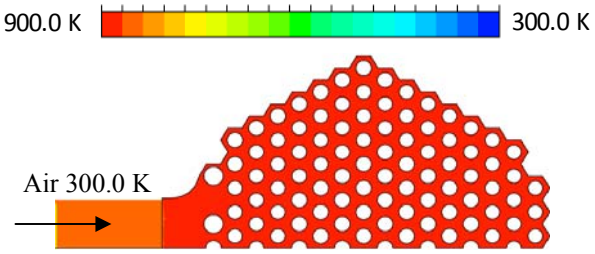

(a) 0.0 sec (T_{avg} = 893.35 K, AMF_{avg} = 0.0)

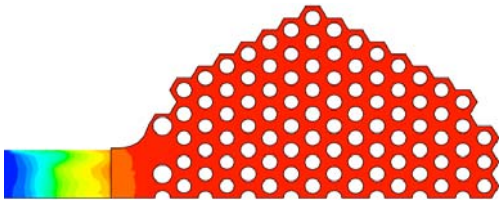

(b) 0.97 sec (T_{avg} = 855.54 K, AMF_{avg} = 0.038)

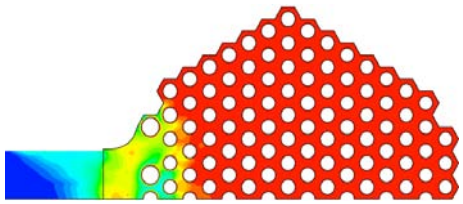

(c) 1.97 sec (T_{avg} = 805.27 K, AMF_{avg} = 0.089)

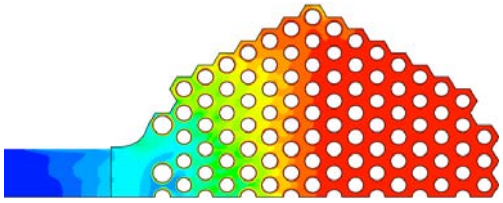

(d) 3.97 sec (T_{avg} = 717.56 K, AMF_{avg} = 0.193)

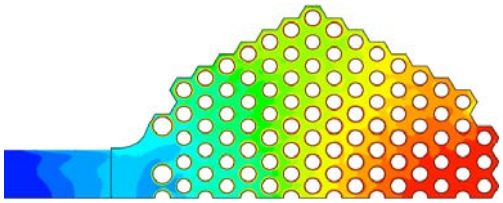

(e) 5.97 sec (T_{avg} = 629.68 K, AMF_{avg} = 0.335)

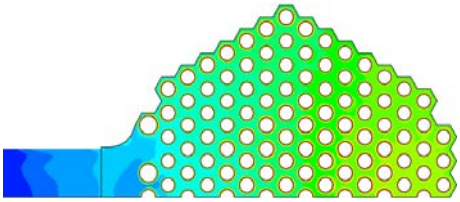

(f) 9.86 sec (T_{avg} = 535.51 K, AMF_{avg} = 0.472)

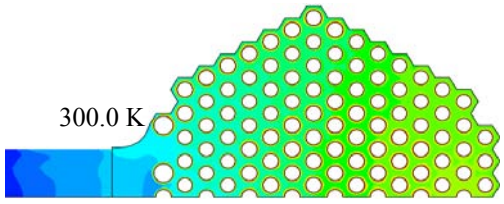

(g) 12.86 sec (T_{avg} = 541.79K, AMF_{avg} = 0.483)

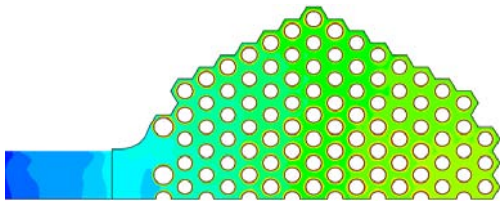

(h) 15.11 sec (T_{avg} = 557.85K, AMF_{avg} = 0.487)

Figure 16. Temperature distribution on the plane of z = 6.7 m in the lower plenum (LP bottom: z = 7.624 m, LP top: z = 7.624 m temperature and air mass fraction are averaged over the area of the plane at z = 6.7 m)

AIR INGRESS MITIGATION

For mitigation of the air-ingress accident, a helium injection method has been proposed and tested by CFD simulations. The simulation was performed by using FLUENT 6.3 code, and the model has been simplified to 2-D geometry. Two different simulations have been performed here for comparisons. One case is no-injection scenario (V_{inj} = 0 m/s) as already shown in the previous sections, and the other case is the helium injection scenario (V_{inj} = 0.5 m/s). In the later simulation, the helium was injected at the bottom of the lower plenum. The size of the injection port was assumed to be 30 cm, and the tested velocity was 0.5 m/s normal to the lower plenum side wall. The temperature of the helium was assumed to be 300 K.

Figure 17 shows the contour plots of the air mass fractions in the reactor and cavity during the air-ingress accident. Figure 17(a) shows the no-injection scenario, and Figure 17(b) shows the helium injection scenario. These figures show that helium injection led to very different air distributions in the core from the no-injection case. The helium injected into the core reduced air concentrations significantly by replacing the air in the core. This is because of the low helium density compared to that of air. In this case, air flow was clearly separated from helium and returned back to the broken hot-leg via recirculation flow.

In contrast, the majority of helium injected into the lower plenum moved into the core and released out of the vessel through the cold-leg. According to the previous air-ingress studies , the upper part of the lower plenum and the lower part of the bottom reflector are shown to be the most seriously corroded and damaged by graphite oxidation because of relatively high temperature and large air concentrations. However, Figure 17(b) shows that the helium injection successfully covers the upper lower plenum and the bottom reflector parts maintaining the air concentration very low at these locations. It indicates that the injection of helium can protect not only the core but also the lower plenum and the bottom reflectors from the serious oxidation damages. For validations of this method for a variety of conditions, further studies are now on going in Idaho National Laboratory.

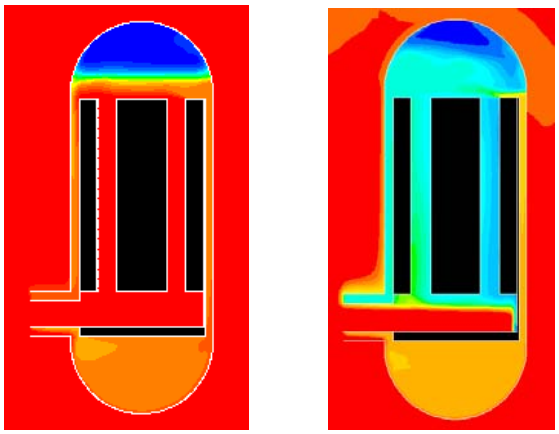

(a) V_{inj} = 0 m/s (200 sec) b) V_{inj} = 0.5 m/s (200 sec)

Figure 17. Effect of helium injection at the lower plenum (Air Mass Fraction).

CONCLUSIONS AND FUTURE STUDIES

The 3-D CFX results of the 3-D DEGB analysis by CFX-12 show that air can actively ingress the reactor vessel because the air inflow momentum generated by the stratified flow and the buoyant flow. This is because heat transfer from the solid structures inside the reactor vessel sufficiently overcome the hydraulic resistance when air passes the lower plenum and core blocks. This confirms that the previous FLUENT 2-D results with the porous media model are reasonable. The expected onset of natural circulation time estimated by 3-D CFX analysis is approximately 100 seconds, which is 50% of that of FLUENT 2-D analysis results.

A supplemental CFD calculation should be performed to confirm the starting time of the air flowing into the core blocks by changing the support block temperature. Several sensitivity calculations should be conducted to reduce the uncertainty of the 3-D CFX results by changing the numerical model for the convection term, the turbulent model, and the reference density value for the buoyant flow. The effect of the reference density value in the buoyant flow should also be carefully examined because the buoyant flow is a main driving force in the air ingress accident and its model is simply calculated by the density difference value based on the reference density value and the gravitational vector.

The qualitative results of the 3-D CFX analysis may not be changed because a lot of the heat structures definitely existed in the lower plenum and the density driven counter-current flow of air and helium is already verified by these experiments.

One case for air ingress mitigation was performed using 2-D CFD code wherein helium was injected from the lower plenum. Preliminary results indicate that helium injections from the lower plenum can protect the core, the graphite structure in the lower plenum, and the bottom reflectors from serious oxidation damage. Air ingress mitigation is being further investigated.

ACKNOWLEDGEMENTS

This work was supported through the Department of Energy's NGNP Project under DOE Idaho Operations Office Contract DE-AC07-99ID13727.

REFERENCES

ANSYS, CFX-12 Manual, 2009.

General Atomics, 1996, *Gas Turbine-Modular Helium Reactor (GT-MHR) Conceptual Design Description Report*, 910720, Rev. 1.

Johnson, R. W., "Modeling Strategies for Unsteady Turbulent Flows in the Lower Plenum of the VHTR," *Nuclear Engineering and Design*, Vol. 238, 2008, pp. 482–491.

Kang, H. S., 2006, "CFD Analysis for the Turbulent Flow in the 3×3 Hybrid Vane," FLUENT User Group Meeting, Kyungju, Korea.

Lowe, R. J., Rottman, J. W., and Linden, P. F., 2005, "The non-Boussinesq lock-exchange problem. Part 1. Theory and experiments," *J. Fluid Mechanics*, Vol. 537, pp.101–124.

Liou, C. P. et al, 2005, "Stratified Flows in Horizontal Piping of Passive Emergency Core Cooling Systems," *13th International Conference on Nuclear Engineering, ICONE 13-50450, May 16–20, Beijing, China*.

Oh, C. H., Kim, E. S., NO, H. C., and Cho, N. Z., 2008, *Experimental Validation of Stratified Flow Phenomena, Graphite Oxidation, and Mitigation Strategies of Air Ingress Accident*, INL/EXT-08-14840, December 2008.